# Adenine nucleobase directed supramolecular architectures based on ferrimagnetic heptanuclear copper(II) entities and benzenecarboxylate anions

Jon Pascual-Colino,[a] Garikoitz Beobide,[a] Oscar Castillo,*,[a] Peter Lodewyckx,[c] Antonio Luque,[a] Sonia Pérez-Yáñez,[b] Pascual Román,[a] and Leticia F. Velasco[c]

[a]Departamento de Química Inorgánica, Facultad de Ciencia y Tecnología, Universidad del País Vasco, UPV/EHU, Apartado 644, 48080 Bilbao, Spain
[b]Departamento de Química Inorgánica, Facultad de Farmacia, Universidad del País Vasco, UPV/EHU, 01006 Vitoria-Gasteiz, Spain
[c]Departament of Chemistry, Royal Military Academy, Renaissancelaan 30, 1000 Brussels, Belgium.

**ABSTRACT:** Two planar organic anions, benzoate and benzene-1,4-dicarboxylate (terephthalate), have been selected as potential π-stacking intercalators among ferrimagnetic $[Cu_7(\mu\text{-adeninato})_6(\mu_3\text{-OH})_6(\mu\text{-}H_2O)_6]^{2+}$ heptameric discrete entities. The resulting supramolecular architecture is highly dependent on the negative charge density distribution, mainly located in the carboxylate groups of the organic anions. In this sense, the benzoate anion, with just one carboxylate group, does not allow its intercalation between the adeninato ligands as it would imply a high steric hindrance among the heptameric entities. As a consequence, these benzate anions are located inside the voids of the crystal structure reducing the accessible volume of compound $[Cu_7(\mu\text{-adeninato})_6(\mu_3\text{-OH})_6(\mu\text{-}H_2O)_6](benzoate)_2\cdot\sim17H_2O$ (**1**). On the contrary, the terephthalate anion, containing two carboxylate groups at opposite sites, adopts a π-stacking sandwich arrangement between two adeninato ligands that affords the porous open structure of formula $[Cu_7(\mu\text{-adeninato})_6(\mu_3\text{-OH})_6(\mu\text{-}H_2O)_6](terephthalate)\cdot nH_2O$ (**2a, 2b**; n: 12 and 24, respectively). In addition to that, the less directional nature of the π-stacking interactions in comparison to the complementary hydrogen bonding based supramolecular metal-organic frameworks (SMOFs), suits them with a flexible architecture able to reversibly adsorb/desorb water (up to a 25-30% at 20ºC) altogether with the expansion/shrinkage of the crystal structure. The bridging adeninato and hydroxido ligands are effective magnetic exchange mediators to provide a $S_T = 5/2$ ferrimagnetic state for the heptanuclear entity.

**Keywords**: π-stacking; adenine; SMOFs; heptanuclear; water uptake; crystal-structure

## 1. INTRODUCTION

Nucleobases are key structure directing agents, as it is well known from the double helix structure of DNA and other biologically relevant systems [1]. Their capacity comes from the rich and diverse combination of hydrogen bond donor and acceptor positions, in many cases close enough to provide complementary hydrogen bonding capability. In this sense, the anchorage of nucleobase to discrete metal-organic entities have been fruitfully employed to build up ordered porous structures known as SMOFs (supramolecular metal-organic frameworks) [2]. SMOFs are compounds that contain potentially accessible voids, in which the 3D crystal building is sustained by supramolecular interactions, mainly hydrogen bonds, as an alternative to the coordination bonds as it happens for the better-known MOFs [3].

However, supramolecular recognition capability of the nucleobases does not lie only on these hydrogen-bonding interactions but also on its ability to establish □-□ stacking interactions. These latter interactions are less directional than the hydrogen bonds but can play a crucial role on the resulting supramolecular architecture. In fact, calculations on the stability of the DNA indicate that these □-□ stacking interactions are crucial to provide stability to the double helix [4].

Therefore, we aimed at getting a deeper insight on the resulting supramolecular assembling coming from the latter interactions. For that purpose, we have selected the rigid and discrete $[Cu_7(\mu\text{-ade})_6(\mu_3\text{-OH})_6(\mu\text{-}H_2O)_6]^{2+}$ (ade: adeninato) entity in which a central $[Cu(OH)_6]^{4-}$ core is coordinated to six external copper(II) metal centers which are further bridged by six μ-adeninato-κ*N3*:κ*N9* ligands and six semicoordinated bridging water molecules. The cationic nature of these discrete entities provides a rich source for novel compounds just by replacing the counterion, as it has been previously

reported when this cationic entity crystallizes with sulphate [5] and nitrate [6] counterions. These inorganic anions lack the capacity to establish □-□ stacking interactions. Consequently, the complex entities assembly by means of □-□ stacking interactions between the nucleobases and due to their rigidity, the resulting crystal packing exhibits a potentially porous supramolecular structure. However as the counterions are located inside the voids of the structure, the accessible volume is highly reduced. Contrarily, if the counterion can be intercalated within the 3D supramolecular architecture, the pores remain accessible. This approach was achieved employing the planar/aromatic theobrominate anion that gave rise to a flexible porous material, in which the organic anions are sandwiched between the □-□ stacking adenines [7]. The structural flexibility taking place in this compound is highly unusual for complementary hydrogen bond sustained porous architectures based on rigid discrete entities [8-11]. The less directional □-□ stacking interactions seem to be the source of this behavior as reported for some other π-stacking sustained structures [5].

In this work, we have selected two planar organic anions, benzoate and benzene-1,4-dicarboxylate (terephthalate), in order to analyze the effect of the charge density distribution on the □-□ stacking interactions and, as a consequence, on the supramolecular architecture. Indeed, the □-□ stacking interaction is usually described as an electrostatic attraction between partial opposite charges located in the interacting molecules [12, 13]. In this case, the cationic nature of the discrete heptameric entity imposes a net positive density on the coordinated adeninato ligands (in spite of their formal anionic nature). This fact favours their interactions with the negative charge density of the organic anion, mainly located on the carboxylate groups. Therefore, depending on the presence of two carboxylate groups (terephthalate) or one (benzoate) the organic anion would be able to be sandwiched between □-□ stacking adenines or

not (Scheme 1). Accordingly, the ligand with just one carboxylate would imply such an approach of the heptameric entities that this option is sterically hindered. As a consequence, the benzoate anions are displaced into the channels reducing the accessible volume. On the contrary, the two carboxylate groups located at opposite sites in the terephthalic anion do not present this steric hindrance and allow a sandwich arrangement of the terephthalic anion between the interacting □-□ stacking adenines. This arrangement provides a more open porous supramolecular structure than that obtained using the benzoate anion, but both of them share the fact that their supramolecular crystal structures are flexible.

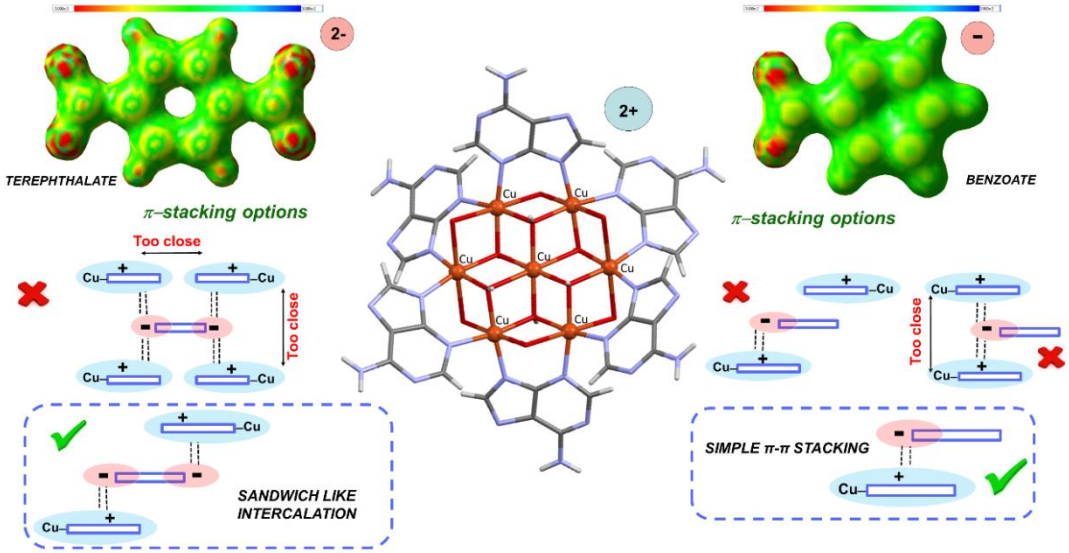


**Scheme 1**. Potential supramolecular π-π stacking interactions between the adeninato ligands and the carboxylate anions.

Keeping all the above in mind, the reaction between copper(II) nitrate, adenine and benzoic (Hbenz) / terephthalic acid ($H_2$tereph) gave rise to the compound [$Cu_7$(μ-ade)$_6$(μ$_3$-OH)$_6$(μ-$H_2O$)$_6$](benz)$_2$·~17$H_2O$ (**1**) and two phases of formula [$Cu_7$(μ-ade)$_6$(μ$_3$-OH)$_6$(μ-$H_2O$)$_6$](tereph)·~n$H_2O$ (**2a, 2b**; n: 12 and 24, respectively) at different states of hydration. Their crystal structures were elucidated by single-crystal X-ray diffraction, allowing to study the supramolecular interactions that direct the crystal building and the

changes taking place during the water adsorption/desorption process. The thermal stability and the magnetic features of these compounds were also analyzed in detail.

## 2. EXPERIMENTAL

### 2.1. Physical measurements

Elemental analyses (C, H, N) were performed on an Euro EA elemental analyzer, whereas the metal content was determined by atomic absorption spectrometer (AAS) from Perkin ElmerAnalyzer 100. The IR spectra were recorded on a FTIR 8400S Shimadzu spectrometer in the 4000−400 $cm^{-1}$ spectral region. Variable-temperature magnetic susceptibility measurements were performed using a standard Quantum Design PPMS magnetometer while cooling from 300 to 2 K at 1kOe. Magnetization as a function of field (H) was measured using the same magnetometer in the $-50 \leq H/kOe \leq 50$ at 2 K after cooling the sample in zero field. The susceptibility data were corrected for the diamagnetism estimated from Pascal's Tables [14], the temperature-independent paramagnetism and the magnetization of the sample holder. Dinitrogen (77 K) and carbon dioxide (273 K) physisorption data were recorded on activated samples (vacuum at 30°C for 6 h) with a Quantachrome Autosorb-iSorb HP1. The measurement conditions have been 40 kV and 40 mA and a sweep between $5< 2\theta < 70º$. Water sorption isotherms of the activated samples were carried out at 20 and 35 ºC using a gravimetric water sorption analyser (Aquadyne DVS, Quantachrome Instruments). Thermogravimetric analyses (TG) were performed on a METTLER TOLEDO TGA/SDTA851 thermal analyzer in synthetic air atmosphere (79% $N_2$/21% $O_2$) with a heating rate of 5°C·$min^{-1}$. Polycrystalline X-ray diffraction data were collected on a PANalytical Xpert PRO diffractometer with Cu−Kα radiation (λ = 1.5418 Å).

2.2. X-ray diffraction data collection and structure determination

Single-crystal X-ray diffraction data were collected on an Agilent Technologies Supernova diffractometer with Cu−Kα radiation (λ = 1.5418 Å) at 298(2) K for compound **1** and an Agilent Technologies Supernova diffractometer with graphite monochromated Mo−Kα radiation (λ = 0.71073 Å) at 293(2) K for **2a** and **2b**. Data reduction was done with the CrysAlisPro program [15]. The details of the structure determination and refinement of compounds are summarized in Table S1. Crystal structure coded **2a** was elucidated from a highly twinned specimen.

All the structures were solved by direct methods using the SIR92 program [16] and refined by full-matrix least-squares on $F^2$ including all reflections (SHELXL97) [17]. All calculations for these structures were performed using the WINGX crystallographic software package [18]. In all cases, some of the adeninato ligands are disordered into two coplanar arrangements with inverted orientation regarding the coordination mode (μ-κ*N3*:κ*N9*/μ-κ*N9*:κ*N3*) [19-21]. In **1** and **2b** these disordered atoms and crystallization water oxygen atoms have been refined with an isotropic temperature factor while the rest of the non-hydrogen atoms of the structure have been modeled with anisotropic temperature factors. In **2a** due to the low quality of the diffraction data, all the atoms not located in the central $Cu_7(OH)_6$ inorganic core were kept with isotropic displacement parameters in order to avoid overparametrization. This procedure also allowed a smoother refinement of the crystal structure that otherwise became very unstable. In all compounds after the initial structure solution was completed, the difference Fourier map showed the presence of substantial electron density at the voids of the crystal structure that was impossible to model. Therefore, its contribution was subtracted from the reflection data by the SQUEEZE method [22] as implemented in PLATON [23].

2.3. Syntheses

2.3.1. Synthesis of $[Cu_7(\mu\text{-ade})_6(\mu_3\text{-OH})_6(\mu\text{-}H_2O)_6](benz)_2\cdot\sim 17H_2O$ (**1**)

0.0489 g (0.2 mmol) of $Cu(NO_3)_2\cdot 3H_2O$ dissolved in 10 mL of water were added to 0.0390 g (0.3 mmol) of adenine dissolved in 15 mL of an aqueous methanolic 1:1 hot solution (50 ºC). The blue solution was basified to pH~8.8 with NaOH while the mixture was continuously stirred. The obtained purple solution was added to 0.1221 g of benzoic acid (1.0 mmol) dissolved in 20 mL of warm water basified with NaOH (pH~8.8). The purple solution was left to evaporate at room temperature and blue single-crystals were obtained after four days. Yield: 60% (based on metal). Anal. Calcd. for $[Cu_7(\mu\text{-ade})_6(\mu_3\text{-OH})_6(\mu\text{-}H_2O)_6](benz)_2\cdot\sim 17H_2O$, $C_{44}H_{86}Cu_7N_{30}O_{33}$ (MW: 2008.15): C 26.32, H 4.31, N 20.92, Cu 22.15; found C 26.10, H 4.35, N 20.97, Cu 22.24%. FTIR (KBr pellets, $cm^{-1}$): 3465w, 3353vs, 3193w, 2944s, 1646vs, 1609w, 1468vs, 1384s, 1337m, 1309s, 1281m, 1187s, 1150s 1028s, 990m, 934m, 803s, 728s, 653s, 568m, 465s. The homogeneity and purity of bulk samples of compound **1** were checked by elemental analysis and powder X-ray diffraction data.

2.4. Synthesis of $[Cu_7(\mu\text{-ade})_6(\mu_3\text{-OH})_6(\mu\text{-}H_2O)_6](tereph)\cdot\sim 12H_2O$ (**2a**) and $[Cu_7(\mu\text{-ade})_6(\mu_3\text{-OH})_6(\mu\text{-}H_2O)_6](tereph)\cdot\sim 24H_2O$ (**2b**)

Compound **2** was obtained by adding to a 10 mL water solution of 0.0488 g of $Cu(NO_3)_2\cdot 3H_2O$ (0.2 mmol), 0.0390 g of adenine (0.3 mmol) dissolved in 15 mL of warm water-methanol mixture (1:1). The resulting solution (pH = 4.0) is basified with NaOH solution to pH~8.8 and later 0.0997 g of terephthalic acid (0.6 mmol) dissolved in 20 mL of water basified with NaOH at 60 ºC is added. In two days a pale blue powder appears corresponding to the formulae $[Cu_7(\mu\text{-ade})_6(\mu_3\text{-OH})_6(\mu\text{-}H_2O)_6](tereph)\cdot\sim 12H_2O$. Yield 40%. Calcd. for $C_{38}H_{70}Cu_7N_{30}O_{28}$ (MW: 1839.97): C

24.80, H 3.83, N 22.84, Cu 24.18; found C 24.72, H 3.78, N 22.76, Cu 24.17 %. Main IR features ($cm^{-1}$; KBr pellets): 3420s, 3200m, 2930s, 1645vs, 1610s, 1504m, 1462s, 1400vs, 1308m, 1192s, 1146s, 933m, 888w, 742m, 657s, 506w.

Blue single-crystals of this compound have been obtained after one month using test tube diffusion technique in which over the aquo-methanolic solution containing the copper(II) nitrate and adenine mixture, an aqueous solution of the terephthalic acid is layered carefully. Depending on the handling of the crystals: storing them under room conditions (**2a**), or directly picking them from the mother liquid (**2b**) specimens at different hydration stages were achieved.

## 3. Results and discussion

All the compounds described below contain, in addition to the corresponding organic anion, a cationic wheel-shaped $[Cu_7(\mu\text{-ade})_6(\mu_3\text{-OH})_6(\mu\text{-}H_2O)_6]^{2+}$ entity in which a central $[Cu(OH)_6]^{4-}$ core is connected to six outer copper(II) metal centers through $\mu_3$-hydroxido bridges in a radial and planar arrangement. The external copper atoms are doubly bridged by water molecules and peripheral adeninato ligands which exhibit a bidentate $\mu$-$\kappa N3$:$\kappa N9$ coordination mode. All the metal centers present an octahedral geometry with the usual Jahn-Teller tetragonal elongation (Table S2-S4 of Supplementary information), which is more pronounced for the external copper(II) atoms than for the inner one because of the rigidity of the heptanuclear entity. The elongation of the external copper atoms is located along the water-metal-hydroxide direction, in such a way the coordinated water molecules, weakly held, have longer coordination bonds than the adeninato ligands. Less pronounced differences are also observed in the central Cu–OH bonds depending whether they are involved in the Jahn-Teller elongation direction or not.

Although the heptameric entity is analogous to that present in the previously reported $[Cu_7(\mu\text{-ade})_6(\mu_3\text{-OH})_6(\mu\text{-}H_2O)_6](theo)_2\cdot\sim 28H_2O$ [7] (theo: anionic form of the theobromine alkaloid) and $[Cu_7(\mu\text{-ade})_6(\mu_3\text{-OH})_6(\mu\text{-}H_2O)_6](NHEt_3)_2(SO_4)_2\cdot nH_2O$ compounds [5], the crystal packing and the thermal stability of each compound show substantial differences owing the molecular features of the selected counterions which lead to different patterns of supramolecular interactions. The crystal building of these previously reported compounds is maintained by a combination of supramolecular π-π stacking and hydrogen bonding interactions in addition to the electrostatic forces taking place between the charges entities. In the sulphate containing compounds, the arrangement of the heptameric entities generates voids where sulphate and triethylammonium counterions are sited, together with the crystallization water molecules. The thermal release of these water molecules collapses the crystal building and the compounds lose their crystallinity during the dehydration process. In the theobrominato compound alkaloid···alkaloid pairs are inserted between the adeninato ligands of the heptameric units to give a ···A···T···T···A··· (A: adeninato, T: theobrominato) sequence of supramolecular π–π interactions which leads to an open-framework with voids representing 37% of the unit cell. Those additional π-π interactions seem to increase the strength of the crystal building as the compound retains its crystallinity up to 300 °C. However, the plasticity of the supramolecular interactions causes a reversible contraction of the porous system after its outgassing, which precludes the adsorption of gas molecules, but allows a complete reversal to the initial open structure upon exposure to a water-saturated atmosphere.

3.1. Compound $[Cu_7(\mu\text{-ade})_6(\mu_3\text{-OH})_6(\mu\text{-}H_2O)_6](benz)_2\cdot\sim 17H_2O$ **(1)**

According to our expectations the planar benzoate anions stablish □-□ stacking interactions with some of the coordinated adeninato ligands. However, as previously

described (Scheme 1), the charge distribution does not allow a propagation of this interaction as the approach of a second adeninato ligand from an adjacent heptameric entity is sterically hindered, and sandwich arrangement of the benzoato anion between two adeninato ligands is not observed. As a consequence, the 3D supramolecular architecture of compound **1** differs greatly from the previously reported theobrominate analogous. In fact, there are not additional □-□ stacking interactions among the adeninato ligands and, instead of that, they are assembled together through quite unusual complementary hydrogen bonds (Table 1). Four of the adeninato ligands of each heptameric entity form a hydrogen bonded $R_2^2(8)$ ring involving the Hoogsteen face of a nucleobase moiety (exocyclic N16 amino group, imidazolic N17 site) and the imidazolic N37 and C38 atoms of an adeninato ligand belonging to an adjacent heptameric entity (Fig. 1). These connections between heptameric units are reinforced with an additional hydrogen bond involving the imidazolic C28–H28 group and the pyrimidinic N21 site of two adjacent heptameric units.

**Table 1**

Structural Parameters (Å, deg) of Hydrogen Bonding Interactions in Compound **1**.[a]

| Hydrogen-bonding interactions[b] | | | |
|---|---|---|---|
| D–H···A | H···A | D···A | D–H···A |
| N16–H16···N37$^{i}$ | 2.35 | 3.05(3) | 139 |
| C38–H38···N17$^{ii}$ | 2.57 | 3.41(2) | 149 |
| C28–H28···N21$^{iii}$ | 2.62 | 3.49(1) | 156 |
| O1–H1···O49A | 1.66 | 2.63(2) | 175 |
| O1w–H11w···O48A$^{ii}$ | 1.75 | 2.61(2) | 167 |
| O3w–H31w···O48A | 1.94 | 2.74(1) | 153 |

[a]Symmetry codes: (i) 1/3+x−y, −2/3+x, 7/3−z; (ii) 2/3+y, 1/3−x+y, 7/3−z; (iii) 4/3−x+y, 2/3−x,−1/3+z. [b]D: donor; A: acceptor.

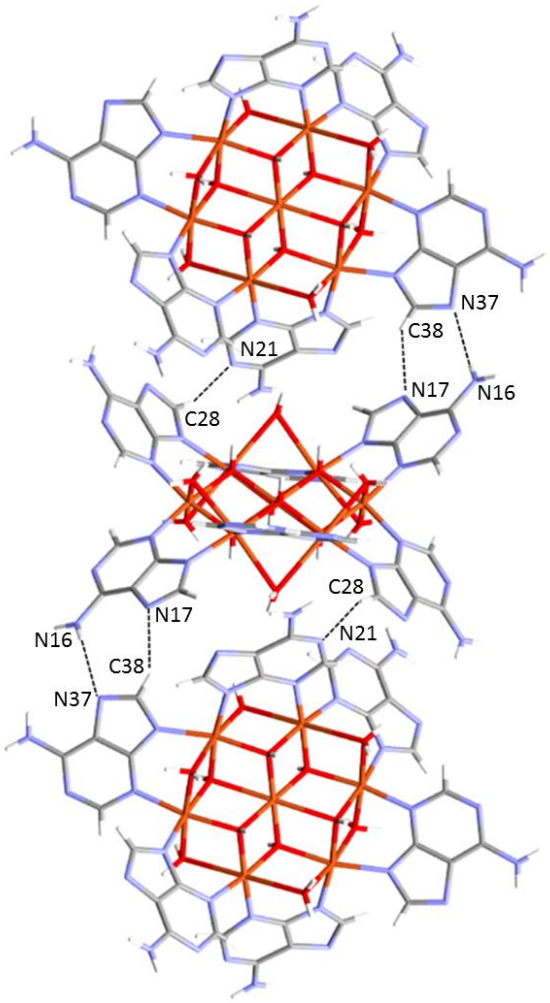


**Fig. 1.** Hydrogen bonding interactions connecting heptanuclear entities in compound **1**.

Considering the above described supramolecular interactions, the 3D arrangement of the complex units can be topologically described as a uninodal 4-connected **nbo**-net, in which the nodes are ascribed to the heptameric units and the linkers correspond to the above described hydrogen bonding interactions [24,25]. This topology, based on the niobium oxide structure, can be also found in one of the first reported bioMOFs in which each paddle-wheel dimeric [$Cu_2$(μ-adeninato)$_4$] unit is linked to four equivalent ones by means of [Cu(oxalate)($H_2O$)] entities leading to a porous coordination polymer [26].

The three dimensional packing in compound **1** allows the occurrence of channels that

are partially occupied by the benzoate anions (Fig. 2) whose phenyl rings are parallel stacked with respect to an adeninato ligand (interplanar distance of 3.60 Å, lateral offset of 1.34 Å). This interaction is reinforced by the presence of hydrogen bonds between the benzoate carboxylate group as acceptor, and one hydroxide group and two coordinated water molecules of neighbouring heptameric units as donors.

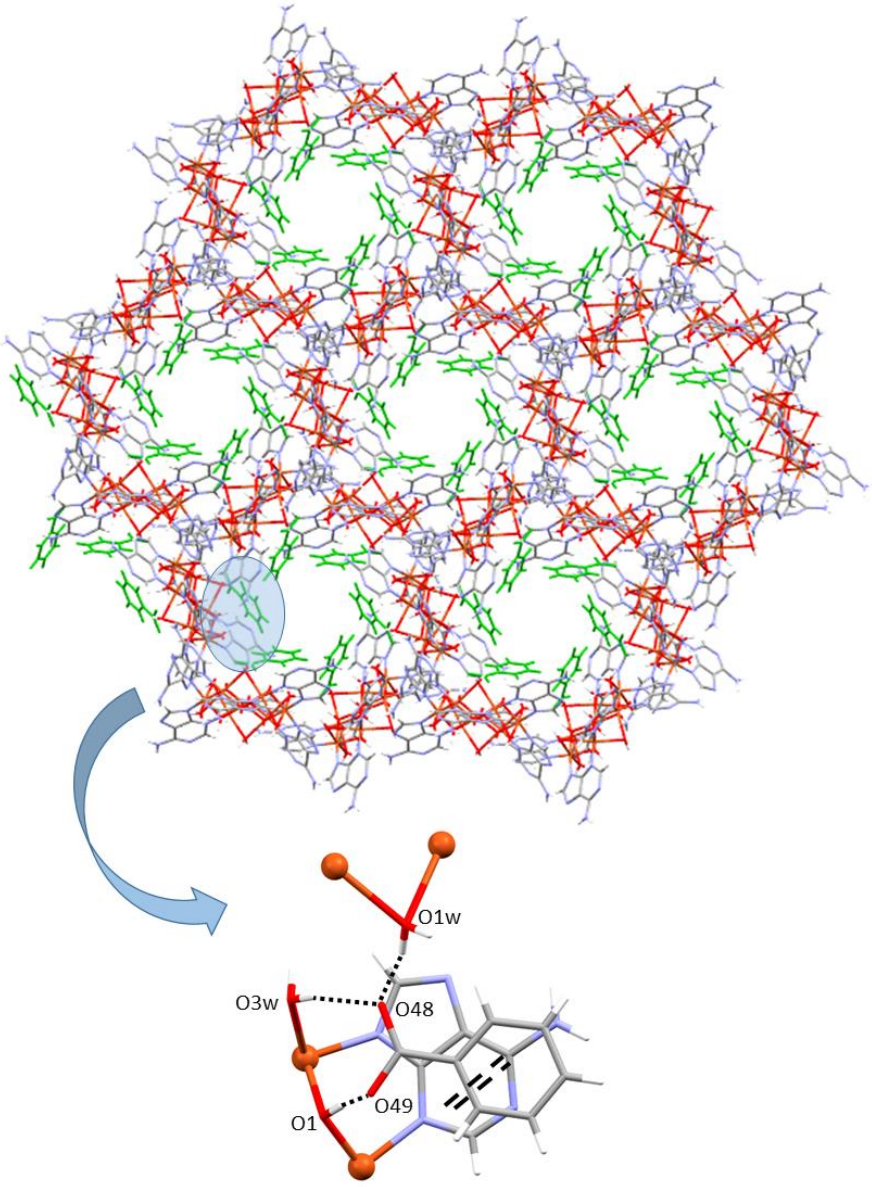


**Fig. 2.** Arrangement of the organic anions (green colour) and the heptameric complex units in compound **1.** Supramolecular benzoate···adeninato interactions are highlighted.

However, the benzoate anions do not completely occlude the channels that run along the crystallographic [001] direction. They present a quite irregular shape with ovoid holes

of a maximum radius of 6 Å (surrounded by the exocyclic N-site of the adeninato ligands) connected through tube-shaped corridors with an approximate radius of 3 Å on whose walls are located the phenyl rings of the benzoate anions (Fig. 2). The volume of these channels, occupied by the crystallization water molecules, is 5098 $Å^3$ (29 % of the total volume of the unit cell as calculated by PLATON). A computational analysis reveals an accessible surface area value of 205 $m^2/g$ and a pore volume of 0.20 mL/g.

The thermogravimetric (Table S5, Fig. S1) and variable-temperature X-ray powder diffraction data of compound **1** (Fig. S2) indicate that under heating it retains the crystallinity but shows a significant structural change after the removal of crystallization (*ca.* 85 ºC) and coordination (*ca.* 160 ºC) water molecules. The shift of diffraction peaks toward higher 2θ angles and the indexation of the variable-temperature X-ray powder diffraction patterns (Figs. S3-S4, Table S6) show a marked and progressive decrease of the unit cell volume from 17812 $Å^3$ for the pristine compound to 13064 $Å^3$ at 85 ºC (loss of the crystallization water molecules). This unit cell shrinkage implies a 93% of the void volume present in the pristine sample (5098 $Å^3$). The loss of coordination water molecules up to 160 ºC only implies an additional decrease of 353 $Å^3$. Accordingly to this sharp void volume reduction, compound **1** is not able to adsorb either $N_2$ at 77 K or $CO_2$ at 273 K. During the outgassing procedure (by vacuuming at 30 °C for 6 h) the colour of compound **1** changes from blue to deep dark green. It undergoes a weight loss mass of 21.0% which fits the expected value for the removal of both crystallization and coordination water molecules (20.6%). The X-ray diffraction pattern of this activated sample (Fig. 3) is equal to that corresponding to the compound heated at 160 °C.

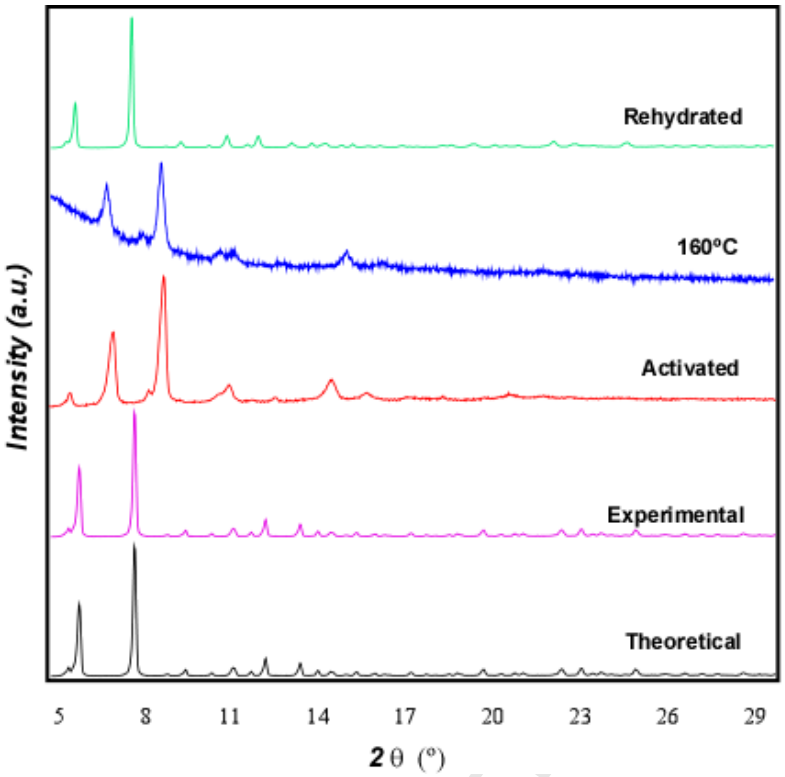


**Fig. 3.** Powder X-ray diffraction patterns from samples of compound **1**.

As previously stated, the dehydration process implies the shrinkage of the pores but the crystal structure is flexible enough to allow the total rehydration of the sample upon exposure to a water-saturated atmosphere for 24 h to recover the original open crystal structure. This behavior is in good agreement with the water vapour adsorption/desorption curves shown in Figure 4.

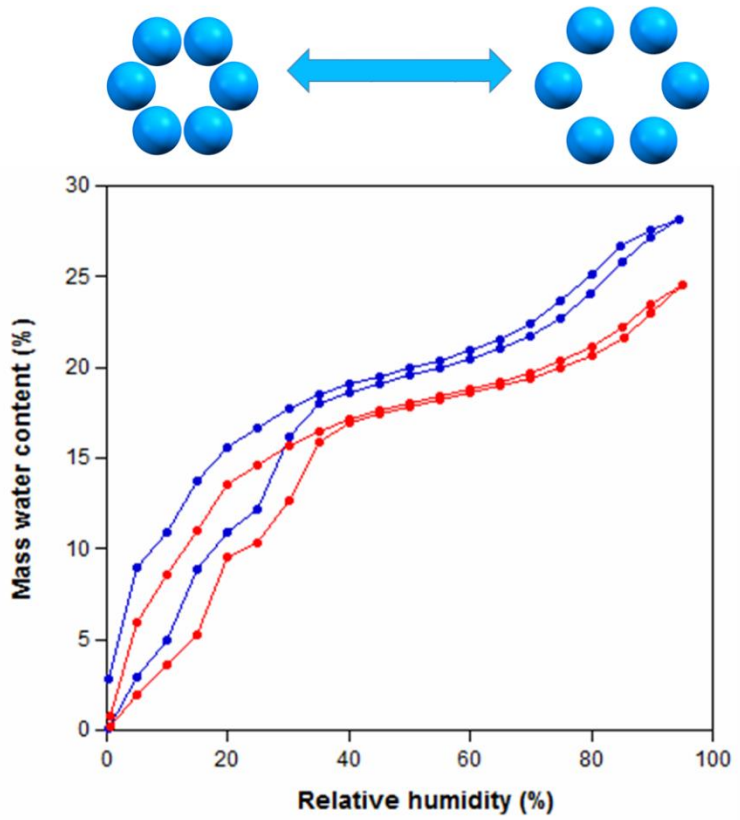


**Fig. 4.** Water vapour adsorption/desorption isotherm for compound **1** at 20 ºC (blue) and 35 ºC (red). Schematic representation of the bottle-neck reversible shrinkage in which the spheres depict the six heptameric units that shrink the pore (top).

The adsorption/desorption isotherms at 20 and 35 ºC of compound **1** show some unusual features such as the presence of three different segments on the adsorption curve: a) a relative increase at low humidity values (0-40%) which corresponds to the adsorption of a water mass content of 19%; b) an apparent plateau at intermediate humidity values (40-60%) with a small increase on the water intake up to 21% and c) a steeper final segment in which water adsorption rapidly increases again with a maximum water uptake of 28% at a relative humidity value of 95%. In addition to that, the desorption curve shows a thin hysteresis at humidity values above 40% that widens noticeably at lower humidity values. These features have been attributed to the flexible nature of the supramolecular architecture. At low humidity values, the pores are essentially collapsed prone to "bottle-neck" like structure for which wide hysteresis

curves are expected. However, as the humidity increases and more water molecules are incorporated into the channels widening them, as a consequence, the "bottle-neck" effect disappears and a thinner hysteresis loop is achieved.

The measurement has been also performed at 35 ºC showing essentially the same features but with a lower amount of water being adsorbed, as expected for a temperature increase. However, it allows, by comparison with the data obtained at 20 ºC, to determine the apparent isosteric adsorption heats (Fig. S5). The values, calculated through Clausius-Clapeyron equation [27], at low coverage value (*ca.* 68 $kJ \cdot mol^{-1}$) compare well with other reported values for MOFs [28-30]. It is important to have in mind that due to the flexible nature of the crystal structure the obtained value does not only reflect the adsorption enthalpy value but also the contribution coming from the structural change that water adsorption implies (apparently of endothermic nature). Therefore, the real isosteric adsorption heat would be probably greater. Many works have pointed out that the presence of strongly polar groups on the surface of the voids help improving the adsorbate-substrate interaction. In this sense, the terephthalate carboxylate groups, the amino group of the adeninato and the hydroxido ligand of this compound point out in this way. This phenomenon has been also reported for other flexible porous materials [31].

3.2. Compounds $[Cu_7(\mu\text{-ade})_6(\mu_3\text{-OH})_6(\mu\text{-}H_2O)_6](tereph)\cdot\sim nH_2O$ **(2a**, **2b).**

The asymmetric unit of compound **2a**, at this stage of hydration, consists of two half centrosymmetric heptameric cations, one terephthalate dianion and twelve crystallization water molecules (Table S7, Fig. S6). The ditopic charge distribution of the therephthlate anion allows its insertion between two adeninato ligands with an interplanar distance of 3.50 Å. Interestingly, the carboxylate groups do not lie just above the adenine aromatic rings but over the adenine chelating ring with the metal

centers where the positive charge density is higher. The anchorage of the organic dianion is reinforced by hydrogen bonds involving its carboxylate oxygen atoms as acceptor and one hydroxide, a coordination water molecule and the exocyclic amino group of the adeninato ligands as donors.

The supramolecular architecture of **2a** is completed by direct N–H···N and C–H···N hydrogen bonding interactions (Table 2) between the adeninato ligands of neighbouring heptameric entities and a strong interaction involving a coordination water molecule as donor and an exocyclic amino group as acceptor (Fig. 5).

**Table 2**

Structural Parameters (Å, deg) of Hydrogen Bonding Interactions in Compound **2a**.[a]

| D–H···A[b] | H···A | D···A | D–H···A |
|---|---|---|---|
| N16–H16B···N31 | 2.47 | 3.25(6) | 151 |
| N56–H56B···N21$^{i}$ | 2.70 | 3.53(5) | 159 |
| C42–H42···N37$^{ii}$ | 2.58 | 3.32(4) | 138 |
| C48–H48···N67$^{iii}$ | 2.60 | 3.36(5) | 139 |
| O5w –H51w···N66$^{iii}$ | 2.09 | 2.85(5) | 149 |
| O1–H1···O771$^{iv}$ | 1.94 | 2.90(3) | 168 |
| O4–H4···O781 | 1.92 | 2.86(3) | 161 |
| O1w–H12w···O772$^{v}$ | 1.80 | 2.71(4) | 161 |
| O2w–H22w···O771$^{iv}$ | 2.55 | 3.43(4) | 160 |
| N66–H66B···O782$^{i}$ | 2.12 | 2.96(4) | 166 |

[a]Symmetry codes: (i) x,−1+y, z; (ii) −1+x, −1 + y, z; (iii) −x, 1−y,−z; (iv) x, 1+y, z; (v) 1− x, 1−y, 1−z. [b]D: donor; A: acceptor.

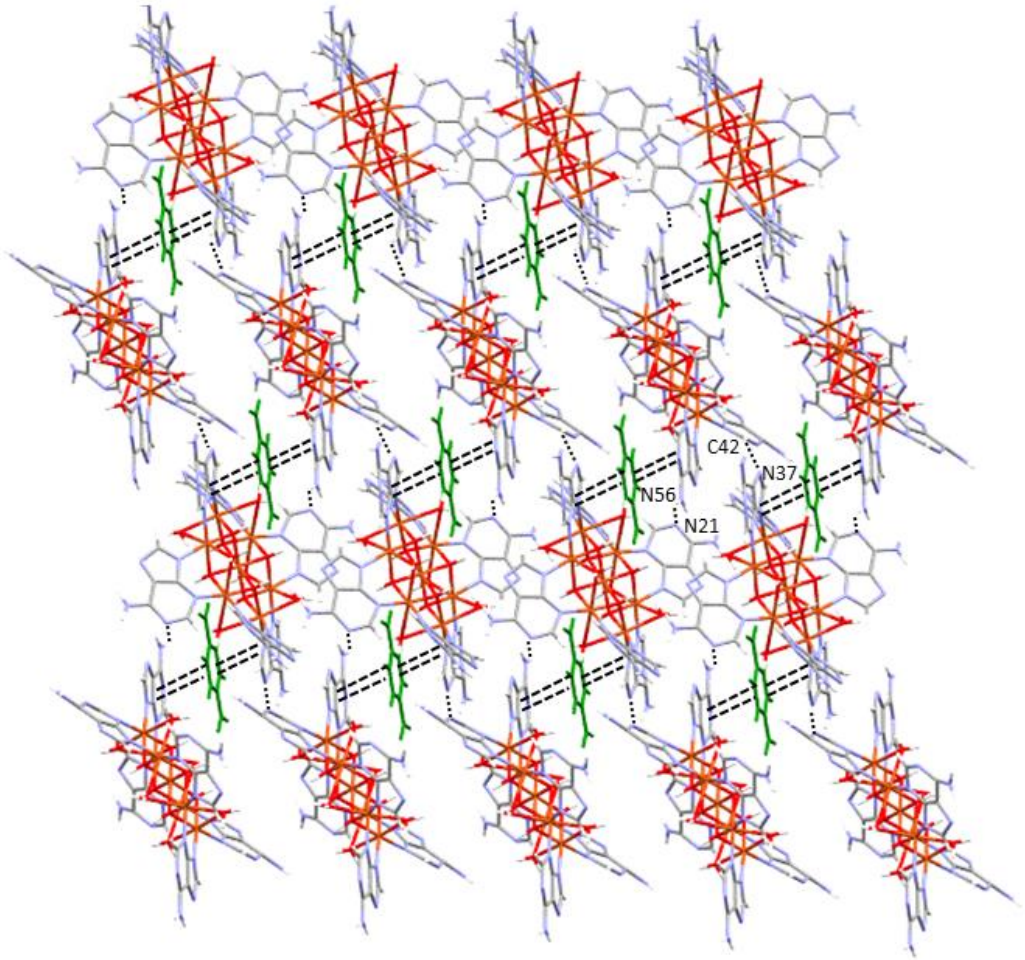


(a)

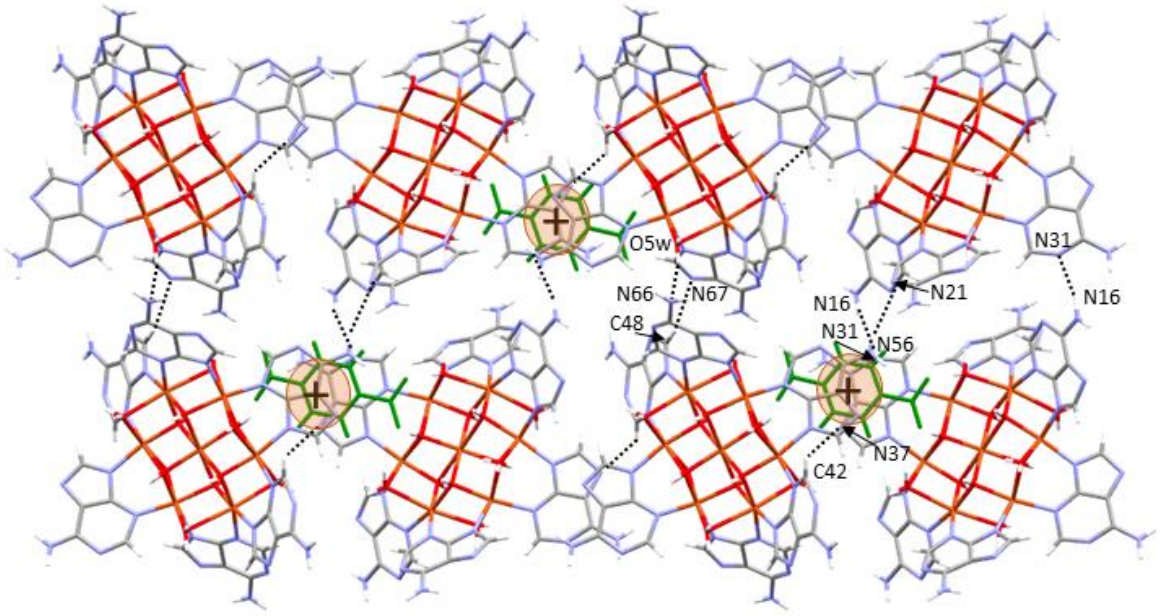


(b)

**Fig. 5. (**a) Crystal packing of compound **2a** along the crystallographic *b*-axis (hydrogen bond: dotted lines; □-□ interaction: double dashed lines) and (b) supramolecular interactions connecting the structural entities (□-□ interaction: + symbol).

The supramolecular assembling of the heptameric entities and the terephthalate anions generates some isolated cavities with a maximum diameter of 4 Å (surrounded by the exocyclic N-site of the adeninato ligands) which are occupied by the crystallization water molecules. The total volume of these voids is the 783 $Å^3$ (22 % of the total volume of the unit cell).

As reported in the synthesis section, a more hydrated phase of terephthalate containing compound has been also structurally characterized (**2b**) which involves the presence of a total of 24 crystallization water molecules inside the channels. The presence of twelve additional water molecules leads to a significant unit cell volume increase (from 3495 to 4142 $Å^3$) and some relevant changes on the supramolecular interactions take place (Fig. 6, Table 3).

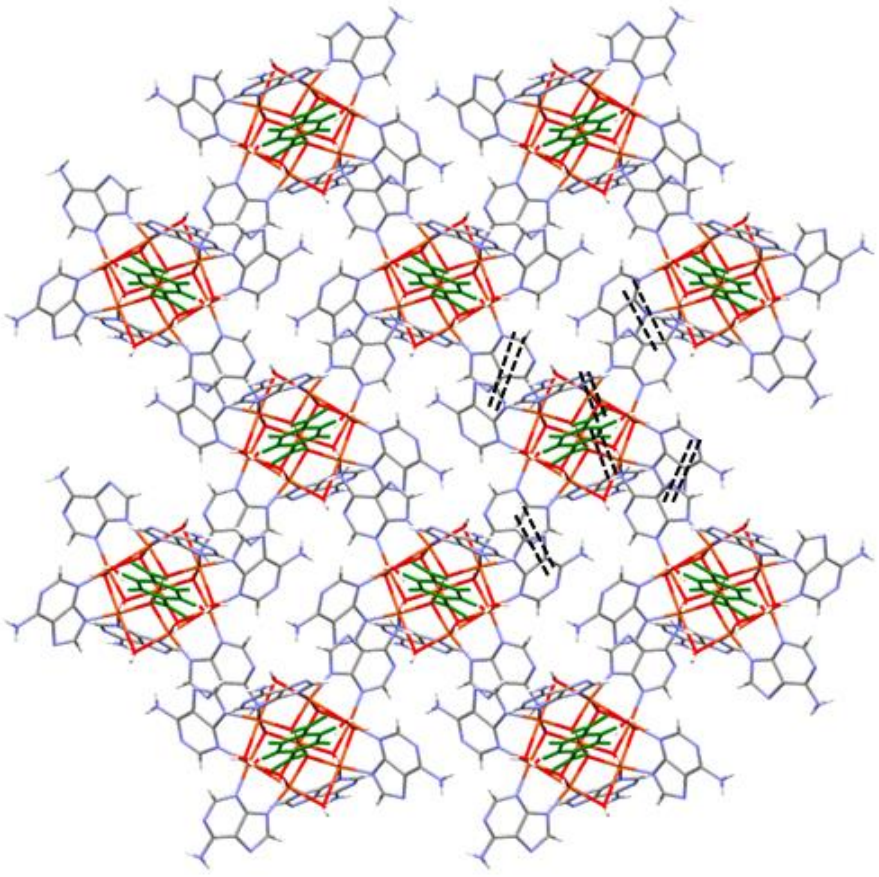

(a)

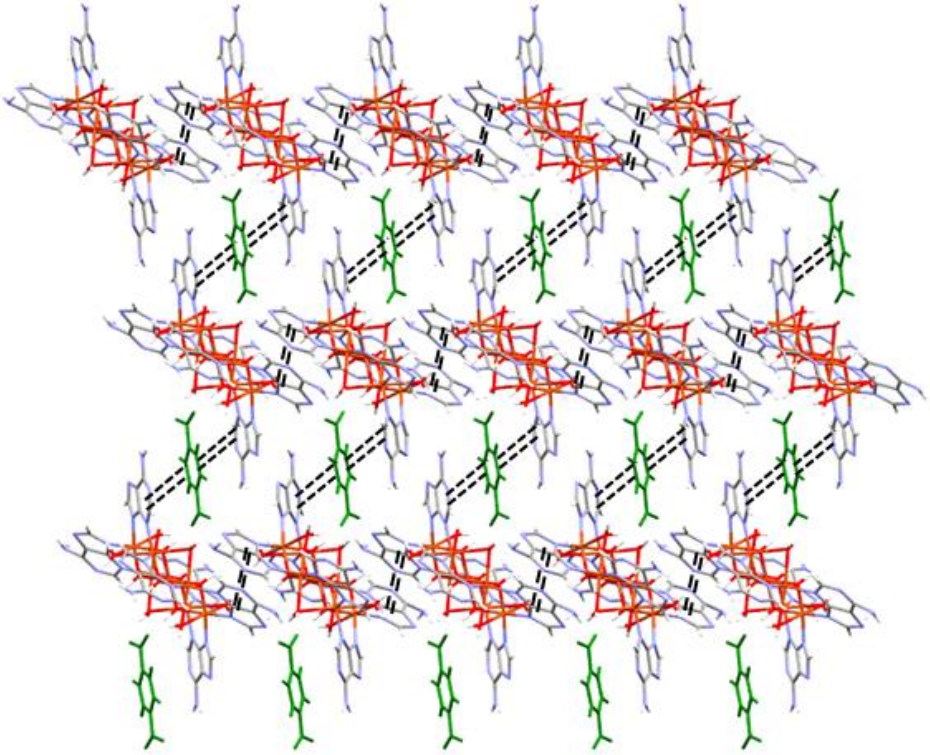

(b)

**Fig. 6.** (a) Layer of heptameric entities in the *bc*-plane of compound **2b**. (b) View along the crystallographic *b*-axis showing the insertion of the organic anion (green colour). Dashed lines represent the □-□ interactions connecting the structural entities.

**Table 3**

Structural Parameters (Å, deg) of Hydrogen Bonding Interactions in Compound **2b**.[a]

| D−H···A[b] | H···A | D···A | D−H···A |
|---|---|---|---|
| O1−H1···N36$^{i}$ | 1.87 | 2.85(2) | 175 |
| O2−H2···O471 | 1.65 | 2.61(2) | 164 |
| O3−H3···O4w | 1.85 | 2.82(2) | 174 |
| O1w−H11w···O9w$^{ii}$ | 1.90 | 2.74(2) | 165 |
| O1w −H12w···O472$^{iii}$ | 1.93 | 2.77(2) | 162 |
| N16A−H16A···O9w$^{iv}$ | 1.97 | 2.81 (3) | 171 |
| O2w−H21w···N31$^{i}$ | 1.98 | 2.80(2) | 158 |
| O2w−H22w···O6w | 1.96 | 2.84(2) | 170 |
| N26B−H26C···O11w$^{v}$ | 2.05 | 2.89(4) | 165 |
| O3w−H32w···O471 | 2.20 | 3.02(2) | 162 |
| N36−H36B···O4w$^{ii}$ | 2.43 | 3.19(2) | 137 |
| C32−H32···O9w$^{ii}$ | 2.50 | 3.40(2) | 163 |

[a]Symmetry codes: (i) 1−x, 1/2+y, 1/2−z; (ii) 1−x, −1/2+y, 1/2−z; (iii) 1−x, −y,1−z; (iv) x,−1/2−y, 1/2+z; (v) −1+x, 1/2−y, −1/2+ z. [b]D: donor; A: acceptor.

The origin of the supramolecular change comes from the competition on the hydrogen bonds of the adeninato ligands being established with the adjacent nucleobases or with the crystallization water molecules. This is not the first case in which the presence of water has disrupted the direct hydrogen bonding interactions between the nucleobases. For example, compounds of formula $[Cu_2(\mu\text{-adenine})_4(Cl)_2]Cl_2\cdot\sim 2CH_3OH$ [10] and $[Cu_2(\mu\text{-adenine})_4(Cl)_2]Cl_2\cdot 6H_2O$ [32] greatly differ in their crystal structure (porous and non-porous, respectively) just due to the presence or not of water solvent molecules.

At low water content, the nucleobases involved in the □-□ stacking interaction with the terephthalate anion are tilted in such a way that they are able to establish direct hydrogen bonds, involving Watson-Crick face, with adjacent adenines (Fig. 7). However, at higher content of water, these interactions break up and the adenines align linearly (they become being related by a symmetry center) to expose the Watson-Crick faces to the water molecules located inside the channels. This subtle modification of the dominating hydrogen bonding interactions is also responsible of the observed crystal system change (from monoclinic to triclinic) and a longer distance between the centroids of the two heptameric units related by these □-□ interactions (14.6 Å vs 12.8 Å).

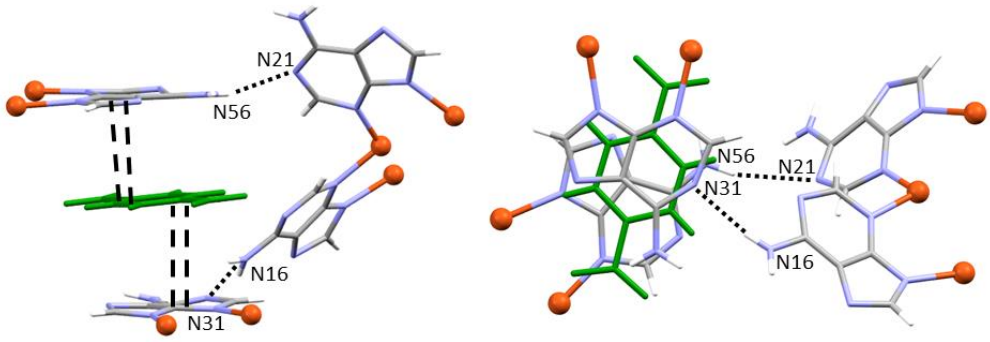


(a)

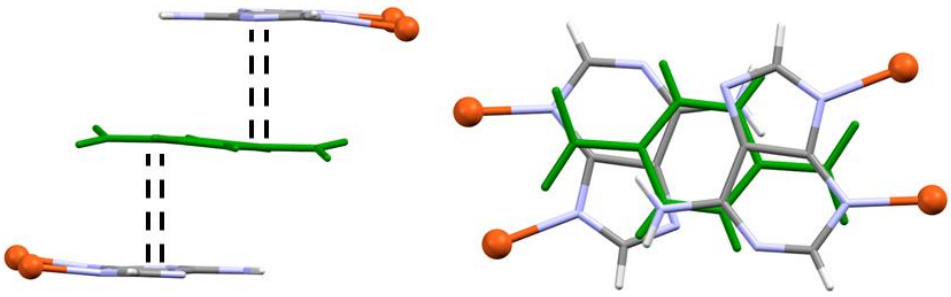

(b)

**Fig. 7.** Arrangement of the terephthalate anion between the adeninato ligands in **2a** (a) and in **2b** (b). Dotted lines indicate hydrogen bonds and double dashed lines represent □-□ interactions.

The resulting supramolecular architecture shows the same bidimensional network described for **2a** but the ovoid holes are greater (7 x 6 Å surrounded by the N-site of the adeninato ligands belonging to heptameric cations) as well as the corridors connecting them with an approximate radius of 3 Å (Fig. 8). The volume of these channels, occupied by the crystallization water molecules, is 1541 $Å^3$ per unit cell (37 % of the total volume as calculated by PLATON). A computational analysis shows an accessible surface area value of 1048 $m^2/g$ and a pore volume of 0.29 mL/g.

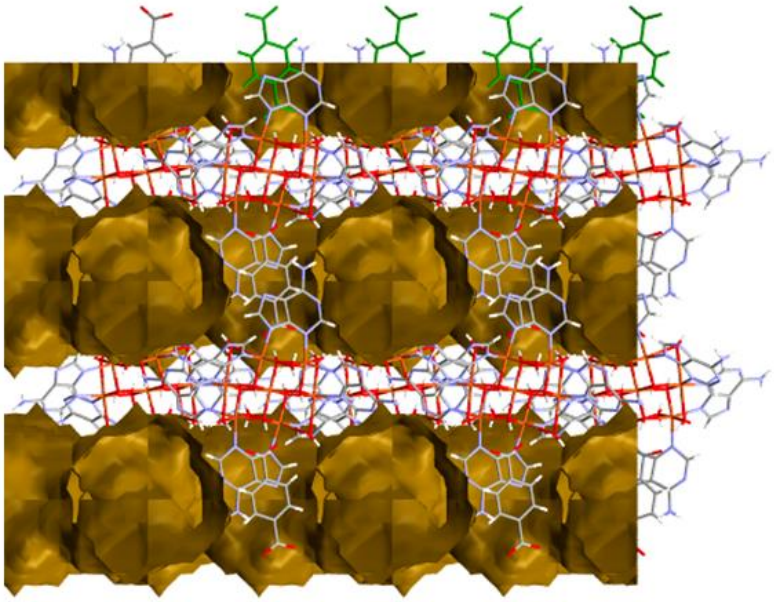

(a)

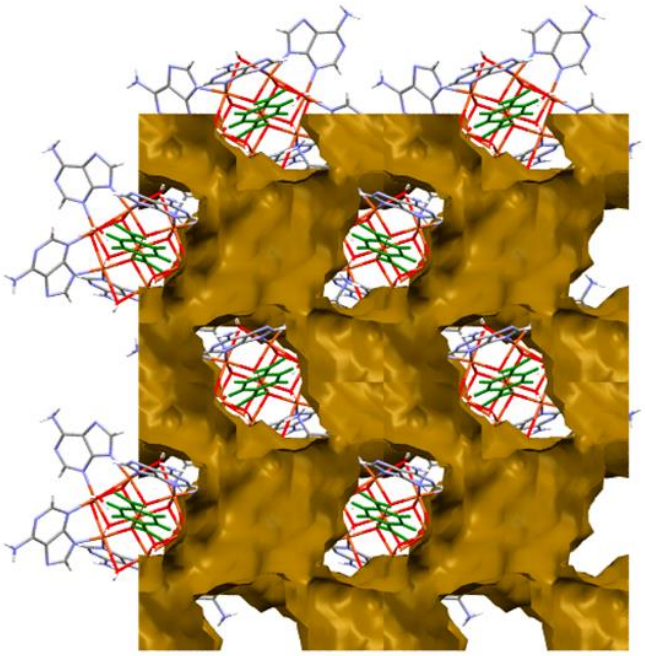

(b)

**Fig. 8.** Views of contact surface of the 2D network of channels in **2b** along the *c*-axis (a) and the *a*-axis (b).

The thermoanalytical and variable-temperature X-ray diffraction data of terephthalate containing compounds show that the release of the crystallization water molecules implies a substantial decrease of crystallinity, as revealed by the widening of the diffraction maxima, which is even more notorious with the loss of coordination water molecules (Table S7 and S8, Fig. S6-S9).

As previously stated, compound **2b** suffers a crystal system change from monoclinic to triclinic during the release of the water molecules. It implies a twining phenomenon of the initial single crystal. In fact, all the crystals selected for the structural characterization were twinned, and all the efforts made for avoiding this twinning were unfruitful. In addition to that, during the water release, the border between the generated domains is getting highly disordered in such a way that they may not be able to come back to the water rich monoclinic phase (**2b**), giving rise to the observed significant amorphization of the sample. In addition, a vacuum activated sample, shows in its X-ray powder diffraction pattern the same loss of crystallinity and a change on the color from

blue to a deep green. This sample was not able to adsorb $CO_2$ (298 K), neither $N_2$ (77 K) but it adsorbed water vapour (Fig. 9). It is notorious the presence of pronounced hysteresis curves that do not close at low humidity values. There is still a 6% of water retained, at zero humidity value, a value close to that expected for the coordination water molecules. Despite the adsorption capacity is reduced after the second cycle the starting first points of the adsorption curve are almost the same up to this value, which implies that the amorphization hindered adsorption capability only applies on the crystallization water molecules but not on the coordination ones. The latter conclusion is also reinforced by the fact that desorption curves finish at the same water content. As stated, the partial amorphization of the sample probably contributes to the pronounced hysteresis loops.

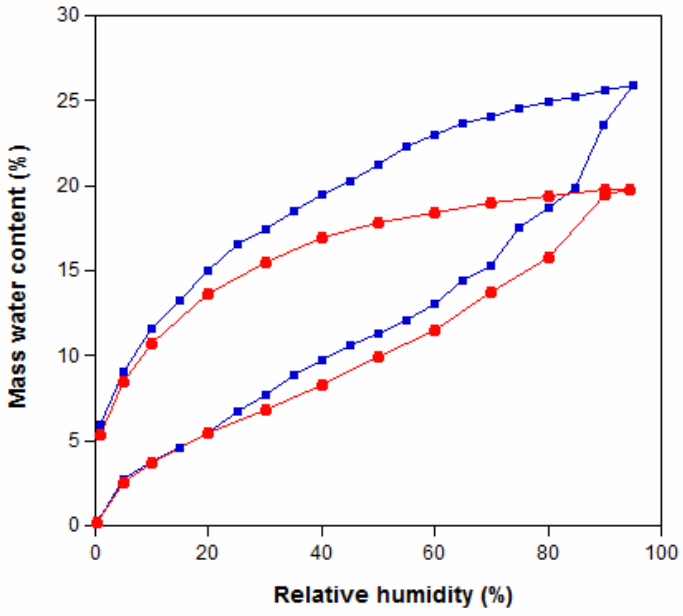


**Fig. 9.** Water cycling of adsorption/desorption isotherms at 20 ºC for an activated sample of compound **2a** (first cycle: blue, second cycle: red).

3.3. Magnetic properties

The magnetic measurements of compounds **1** and **2** indicate an overall ferrimagnetic behavior within the heptameric copper-adenine entity (Fig. 10). The $\chi_M T$ value at room temperature agrees with the expect value for seven paramagnetic copper(II) metal

centers. This value remains basically constant upon cooling and only at temperatures below 100 K starts deviating towards higher values to achieve a maximum of 4.85 $cm^3$ K $mol^{-1}$ and 5.09 $cm^3$ K $mol^{-1}$, respectively. The magnetization curve at 2 K shows a linear dependence, from 0 to 12−15 kOe, which slowly tends to saturate to a value of 5.22 and 5.53 $\mu_B$/heptamer at 20 kOe. These values which agree with the presence of a central copper(II) metal center antiferromagnetically coupled to the six external ones [5] to provide a $S_T = 5/2$. The magnetization curve shows no hysteresis, indicating that the magnetic contributions are limited to the molecular scale of the heptameric entity without providing a 3D ordering. Only at very low temperature in the $\chi_M T$ curve, it can be observed a slight decrease probably due to the presence of very a antiferromagnetic interheptameric coupling mediated through the supramolecular interactions.

Taking into account the molecular structure of the $[Cu_7(\mu\text{-ade-}\kappa N3{:}\kappa N9)_6(\mu_3\text{-OH})_6(\mu\text{-}H_2O)_6]^{2+}$ heptanuclear entity present in both compounds and the Jahn-Teller elongated octahedron of the central copper(II) atom, the following Hamiltonian (Equation 1) was employed to fit the experimental data.

$$H = -J_1\left(\vec{S}_1\cdot\vec{S}_3+\vec{S}_1\cdot\vec{S}_4+\vec{S}_1\cdot\vec{S}_{3'}+\vec{S}_1\cdot\vec{S}_{4'}\right)-J_2\left(\vec{S}_1\cdot\vec{S}_2+\vec{S}_1\cdot\vec{S}_{2'}\right) - J_3\left(\vec{S}_2\cdot\vec{S}_3+\vec{S}_3\cdot\vec{S}_4+\vec{S}_4\cdot\vec{S}_{2'}+\vec{S}_{2'}\cdot\vec{S}_{3'}+\vec{S}_{3'}\cdot\vec{S}_{4'}+\vec{S}_{4'}\cdot\vec{S}_2\right)-g\mu_B\vec{B}\cdot\vec{S} \quad \text{(equation 1)}$$

$J_1$ and $J_2$ couplings are assigned to the superexchange interactions between the central and the external copper ions taking place through double μ-OH and μ-O bridges. $J_1$ involves a mixture of short-short and short-long distances. $J_2$ presents only a short-short Cu–O based arrangement. $J_3$ represents the superexchange interaction between the external $Cu^{II}$ ions.

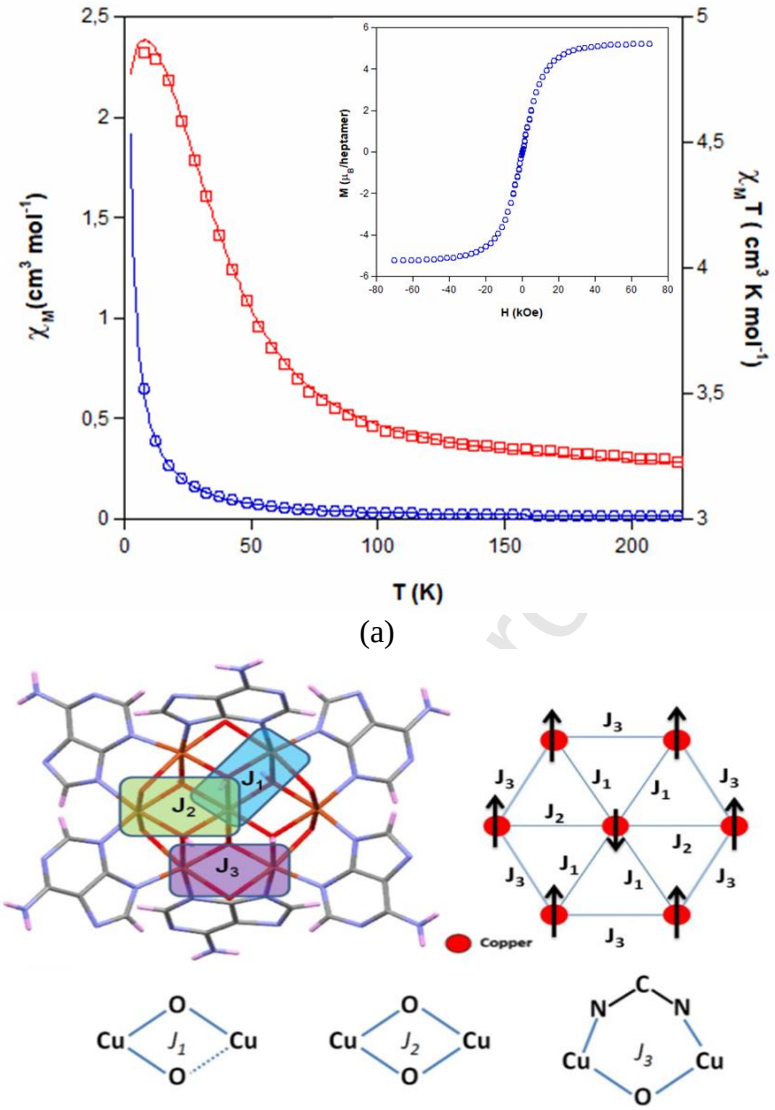


**Fig. 10.** (a) Thermal evolution of the molar magnetic susceptibility $\chi_m$ (o) and $\chi_m T$ (□) product for compound **1**. Magnetization curve at 2 K (inset). The line shows the best fitting of the experimental data. (b) Magnetic scheme of $[Cu_7(\mu\text{-ade-}\kappa N3{:}\kappa N9)_6(\mu_3\text{-}OH)_6(\mu\text{-}H_2O)_6]^{2+}$ heptanuclear entity emphasizing the different relationships of the magnetic topologies and 3-J coupling types for the local $Cu^{II}_7$ cluster.

The fitting of the $\chi_m T$ experimental data to this model was performed using the MagProp software tool distributed with DAVE [33]. The best fitting parameters (see the red continuous line in Figure 10a and Figure S11) are $J_1$ = -2, $J_2$ = -100, $J_3$ = 67 $cm^{-1}$ and g = 2.13 for compound **1** and $J_1$ = 35, $J_2$ = -180, $J_3$ = 100 $cm^{-1}$ and g = 2.11 for compound **2a**. This behavior and the obtained superexchange values are similar to those published for other similar whell-shaped copper(II) heptameric entities in which the

outer metal atoms are ferromagnetically coupled to each other and antiferromagnetically coupled to the central atom [5, 6].

## 4. CONCLUSIONS

These compounds have proved that the features of the nucleobases that make them so well suited to deliver a stable complex structure such as those of DNA/RNA, upon which life has evolved, prompt them also as useful tools to develop ordered supramolecular materials. The present work implies the generation of porous materials in which subtle changes such as the negative charge density distribution on simple organic carboxylate anions provides rather different supramolecular architectures. Additionally, the π-stacking interaction mode of the adenines provides flexible structures that response under external stimuli such as the atmosphere humidity. The strong hydrogen bonding capacity of the water guest molecule seems to be the key for the structural reversibility as their interaction with the host inner-surface must compensate the rupture of some direct hydrogen bonding interactions between the nucleobases that are only present in the collapsed crystal structures. The coordination mode of the adeninato ligands also facilitates magnetic interactions that lead to a ferrimagnetic material in this case. It all envisages a fruitful future for the development of metal-organic materials based on so ubiquitous biological molecules.



## Declaration of Competing Interest

The authors declare that there is no conflict of interest.

## Acknowledgements

This work has been funded by Universidad del País Vasco/Euskal Herriko Unibertsitatea (PPG17/37, predoctoral PIF17/051 fellowship for J.P.C.), Gobierno Vasco/Eusko Jaurlaritza (PIBA18-59 and IT1291-19) and Ministerio de Economía y Competitividad (MAT2016-75883-C2-1-P). Technical and human support provided by SGIker (UPV/EHU, MICINN, GV/EJ, ESF) is also acknowledged. In memoriam of

Professor Juan Manuel Salas Pelegrín and his contribution to the research on bioinorganic chemistry in Spain.

AUTHOR INFORMATION

**Corresponding Author**

e-mail: oscar.castillo@ehu.eus

REFERENCES


(1) E. Chargaff, In The Nucleic Acids vol.1, p. 308, E. Chargaff & J. N. Davidson, AcademicPress, New York, 1955.

(2) S. Pérez-Yáñez, G. Beobide, O. Castillo, J. Cepeda, A. Luque, Nova Science Publishers, Inc. pp 67–92, 2016.

(3) H.C. Zhou, J.R. Long, O.M. Yaghi, Chem. Rev. 112 (2012) 673−674.

(4) P. Yakovchuk, E.Protozanova, M.D. Frank-Kamenetskii, Nucleic Acids Research 34 (2006) 564–574.

(5) R. Pérez-Aguirre, G. Beobide, O. Castillo, I. De Pedro, A. Luque, S. Pérez-Yáñez, J. Rodríguez Fernández, P. Román Inorg. Chem. 55 (2016) 7755–7763.

(6) B.J.M. Leite Ferreira, P. Brandão, A.M. Dos Santos, Z. Gai, C. Cruz, M.S. Reis, T.M. Santos, V. Félix, J. Coord. Chem. 68 (2015) 2770-2787.

(7) J. Pascual-Colino, G. Beobide, O. Castillo, I. da Silva, A. Luque, S. Pérez-Yañez, Cryst. Growth Des. 18 (2018) 3465−3476.

(8) P.S. Nugent, V.L. Rhodus, T. Pham, K.A. Forrest, L. Wojtas, B. Space, M. J. Zaworotko J. Am. Chem. Soc. 135 (2013) 10950-10953.

(9) W. Gong, D. Chu, H. Jiang, X. Chen, Y. Cui, Y. Liu Nature communications 10 (2019) 1-9.

(10) J. Thomas-Gipson, G. Beobide, O. Castillo, J. Cepeda, A. Luque, S. Pérez-Yáñez, A. T. Aguayo, P. Román, CrystEngComm 13 (2011) 3301–3305.

(11) J. Thomas-Gipson, G. Beobide, O. Castillo, M. Fröba, F. Hoffmann, A. Luque, S. Pérez-Yáñez, P. Román, Cryst. Growth Des. 14 (2014) 4019–4029.

(12) C. R. Martinez, B. L. Iverson Chem Sci. 3 (2012) 2191-2201

(13) P. Cysewsky, Phys. Chem. Chem. Phys. 10 (2008) 2636-2645.

(14) A. Earnshaw, Introduction to Magnetochemistry, Academic Press, London, 1968.

(15) CrysAlisPRO, Oxford Diffraction /Agilent Technologies UK Ltd, Yarnton, England.

(16) A. Altomare, G. Cascarano, C. Giacovazzo, A. Guagliardi, M. C. Burla, G. Polidori & M. Camalli, J. Appl. Cryst. 27 (1994) 435.

(17) G. M. Sheldrick, Acta Cryst. C71 (2015) 3–8.

(18) L. J. Farrugia, J. Appl. Cryst. 45 (2012) 849–854.

(19) J. Cepeda, O. Castillo, J.P. García-Terán, A. Luque, S. Pérez-Yáñez, P. Roman, Eur. J. Inorg. Chem. 16 (2009), 2344–2353.

(20) E. Sletten, Acta Crystallogr. B25 (1969) 1480–1491.

(21) E. Sletten, Acta Crystallogr. B26 (1970) 1609–1614.

(22) P. Van der Sluis, A.L. Spek, Acta Crystallogr. A A46 (1990) 194–201.

(23) A.L. Spek, Acta Cryst. D65 (2009) 148-155.

(24) Topos Main Page http://www.topospro.com (accessed: 2019/05/10).

(25) V. A. Blatov, A. P. Shevchenko and D. M. Proserpio, Cryst. Growth Des. 14 (2014) 3576–3586.

(26) J. P. García-Terán, O. Castillo, A. Luque, U. García-Couceiro, P. Román and L. Lezama, Inorg. Chem. 43 (2004) 4549–4551.

(27) O.L.I. Brown J. Chem. Educ. 28 (1951) 428.

(28) H. Furukawa, F. Gándara, Y.-B. Zhang, J. Jiang, W. L. Queen, M. R. Hudson, O. M. Yaghi J. Am. Chem. Soc. 136 (2014) 4369–4381.

(29) H. Kim, H. J. Cho, S. Narayanan, S. Yang, H. Furukawa, S. Schiffres, X. Li, Y.-Biao Zhang, J. Jiang, O. M. Yaghi, E.N. Wang Scientific Reports 6 (2016) 19097.

(30) J. Canivet, A. Fateeva, Y. Guo, B. Coasne, D. Farrusseng Chem. Soc. Rev. 43 (2014) 5594.

(31) N.C Burtch, H. Jasuja, K.S. Walton Chem. Rev. 114 (2014) 10575–10612.

(32) P. De Meester, A.C. Skapski J. Chem. Soc. A A13 (1971) 2167–2169.

(33) R. T. Azuah, L.R. Kneller, Y. Qiu, P.L.W. Tregenna-Piggott, C.M. Brown, J.R.D. Copley, R.M. Dimeo, J Res Natl Inst Stand Technol. 114 (2009) 341–358.

## GRAPHICAL ABSTRACT

Adenine directed π-π stacking interactions guide the supramolecular architectures based on ferrimagnetic heptnuclear Cu(II) entities. These materials follow our attempts in the quest for supramolecular metal-organic frameworks (SMOFs).

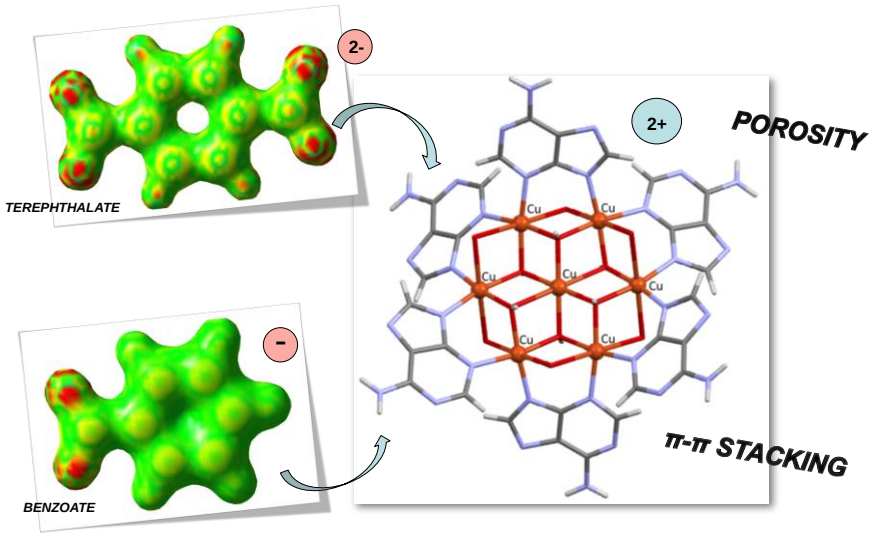

## HIGHLIGHTS

- Adenine nucleobase as powerful tool for the design of porous materials
- SMOFs built up from π-stacking intercalators and metal-nucleobase based heptanuclear entities
- Influence of the negative charge density distribution of carboxylate anions in the structure
- Flexible crystal structures as atmosphere humidity adsorbents
- Ferrimagnetic heptameric entities